Title
Two-dimensional and 3-dimensional optical coherence tomographic imaging of the airway, lung, and pleura

Journal
Journal of Thoracic and Cardiovascular Surgery, 129(3)

ISSN
0022-5223

Authors
Hanna, N
Saltzman, D
Mukai, D
et al.

Publication Date
2005-03-01

DOI
10.1016/j.jtcvs.2004.10.022

Evolving Technology

Two-dimensional and 3-dimensional optical coherence tomographic imaging of the airway, lung, and pleura

N. Hanna, BS,[a] D. Saltzman, MD, PhD,[c] D. Mukai, BS,[a,b] Z. Chen, PhD,[a2] S. Sasse, MD,[c] J. Milliken, MD,[d] S. Guo, PhD,[a] W. Jung, MS,[a] H. Colt, MD,[b] and M. Brenner, MD[a,b]

Ms Hanna

One figure is available online.

From Beckman Laser Institute,[a] University of California, Irvine, Irvine, Calif; the Pulmonary and Critical Care Division[b] and Cardiothoracic Surgery,[d] UC Irvine Medical Center, Orange, Calif; and Veterans Administration Medical Center,[c] Long Beach, Calif.

Supported by the Department of Defense (FA 9550-04-1-0101) and Philip Morris USA grant no. 32598.

Read at the Thirtieth Annual Meeting of The Western Thoracic Surgical Association, Maui, Hawaii, June 23-26, 2004.

Received for publication June 22, 2004; revisions received Oct 7, 2004; accepted for publication Oct 15, 2004.

Address for reprints: Matt Brenner, MD, Pulmonary and Critical Care Division, UC Irvine Medical Center, Bldg 53, Rm 119, 101 City Drive South, Orange, CA 92868 (E-mail: mbrenner@uci.edu) and Zhongping Chen, PhD, Department of Biomedical Engineering, Beckman Laser Institute, UC Irvine, Irvine, CA 9261 (E-mail: Zchen@bli.uci.edu).

J Thorac Cardiovasc Surg 2005;129:615-22

0022-5223/$30.00

doi:10.1016/j.jtcvs.2004.10.022

Background: Methods for obtainingreal-time in vivo histologic resolution by means of noninvasive endoscopic optical imaging would be a major advance for thoracic surgical diagnostics and treatment. Optical coherence tomography is a rapidly evolving technology based on near-infrared interferometry that might provide these capabilities. The purpose of this study is to investigate the feasibility of real-time 2- and 3-dimensional optical coherence tomographic imaging of airway, pleural, and subpleural lung tissues in normal, inflammatory, and malignant animal models and patients with known or suspected airway malignancy.

Methods: Freshly excised lungs and pleural tissue obtained from rabbits with inhalation lung injury and induced empyema, metastatic sarcomas, and pleural sarcomas and from patients with airway disease were imaged by using 2- and 3-dimensional optical coherence tomography with a prototype superluminescent diode optical coherence tomographic system constructed in our laboratory. Lungs and pleural tissue were subsequently processed for standard hematoxylin and eosin histology for comparison with optical coherence tomography.

Results: Optical coherence tomographic imaging achieved an ex vivo resolution of 10 μm and an in vivo resolution of about 30 μm with a depth penetration of 1 to 2 mm with 2- and 3- dimensional reconstruction capabilities. Tumors as small as 500 μm were detectable with optical coherence tomography. The acquired images closely matched histologic images, demonstrating details at the level of mucosal layers, glands, alveoli, and respiratory bronchioles.

Conclusions: Optical coherence tomography with near-infrared interferometric methods enables near real-time in vivo near-histologic resolution optical imaging. With further advances, optical coherence tomography has the potential for real-time accurate and early pleural and subpleural diagnostics by using small-diameter flexible fiberoptic endoscopic probes for a wide range of thoracic surgical applications.

ET

During bronchoscopy or endoscopy or while in the operating room, the ability to distinguish benign from malignant disease and to determine the extent of lesion margins is critical for successful interventions. In addition, rapid and accurate evaluation of airway pathologic changes is important for minimizing morbidity and mortality in other conditions, such as acute burn or inhalation injury.[1,2] Until now, assessment for proper clinical management relied primarily on visualization of abnormalities during endoscopic biopsy on frozen sections sent to pathology and gross inspection at the time of surgical intervention. A means to

obtain real-time noninvasive histologic imaging would aid in diagnosis, help to ensure higher-yield biopsy samples, potentially save considerable operating time, and possibly help avoid unnecessary interventions or repeated procedures.

Optical coherence tomography (OCT) is emerging as a rapid-acquisition, high-resolution imaging modality that provides capabilities for real-time near-histologic evaluation.[3] In attempting to approach the concept of optical biopsy,[4] OCT offers the potential for surface and subsurface optical imaging (up to a depth of 1-2 mm) with high spatial resolution of tissue microstructure without requiring contact between the optical probe and the tissue sample.[3] Tissue layers, glands, small blood vessels, and cartilage can be visualized at theoretic resolutions approaching 10 μm with the use of superluminescent diode (SLD) laser prototype systems.[5] This technology, in combination with minimally invasive techniques, can be applied in the surgical field to examine tissue microstructure, guide biopsies, and minimize the need for frozen sections or the uncertainties associated with gross examination.[6] Additionally, multiple sequential high-resolution images can be captured, rendered, and integrated to form 3-dimensional images.[7]

We developed a fiberoptic OCT probe (1 mm in diameter) for bronchoscopic and thoracoscopic application to assess the feasibility of OCT imaging in inflammatory and neoplastic changes of the airway and lung parenchyma, as well as of visceral and parietal pleural tumors, induced by a novel pleural malignancy animal model developed in our laboratory. Two- and 3-dimensional OCT images were constructed. This technology was then applied to patients with known or suspected airway malignancy.

ET

Materials and Methods

Animal Preparation

Anesthesia and intubation. Male New Zealand White rabbits (Myrtle Rabbitry Inc, Thompson Station, Tenn) weighing 4.0 $\pm$ 0.4 kg were anesthetized with a ratio of ketamine HCI (100 mg/mL, Ketaject; Phoenix Pharmaceutical Inc, St Joseph, Mich) and xylazine (20 mg/mL, Anased; Lloyd Laboratories, Shenandoah, Iowa) at a dose of 0.75 mL/kg administered intramuscularly. Maintenance anesthesia was administered (0.3 mL of a 1:1 mixture of ketamine/xylazine) through the marginal ear vein. Animals were intubated with a 3.0 endotrachael tube and mechanically ventilated (Harvard Apparatus dual-phase control respirator, South Natick, Mass). Animal protocols were approved by the Animal Research Committee (IACUC no. 2001-2272 and 2002-2397).

Airway injury and empyema induction. Twelve animals were inoculated with 1.9×10^3 to 2.4×10^5 *Streptococcus pneumoniae* cells by using a sterile pediatric suction catheter in accordance with an approved protocol from the Institute of Surgical Research, San Antonio, Tex.[8] Animals were monitored on the basis of vital signs, blood work, and pulmonary function tests at the time of and after 24, 48, 72, and 96 hours of exposure. Computed tomographic scans, flow cytometry, and bronchoalveolar lavage fluid culture were performed to confirm the diagnosis of pneumonia. On the fourth day after inoculation, surviving rabbits were sacrificed, and their tracheas were excised, placed in isotonic saline, packed on ice, and sent overnight to the Beckman Laser Institute. All samples were imaged within 3 days of excision. Empyemas were induced in a New Zealand White rabbit, as previously described.[9] In brief, 2 mL of 10^8 *Pasteurella multocida* bacteria (in 0.5% Brain Heart Infusion agar) was injected into the right pleural space. Twenty-four hours after induction, pleural fluid from a diagnostic thoracentesis was cultured and analyzed for pH and glucose to verify the presence of empyema. After day 6 of induction and after the animals were sacrificed, the thorax was dissected en bloc, and specimens from the right middle lobe with attached visceral pleura were collected. These specimens were frozen at -20°C until the time of OCT imaging.

Pleural and parenchymal tumor implantation. After intubation, a 4-mm thoracoscope (Karl Storz, Tuttlingen, Germany) was inserted under sterile conditions in the fifth or sixth intercostal spaces of 12 New Zealand White rabbits, and with thoracoscopic visualization, a small section of the chest wall parietal pleura was mildly abraded with the wooden end of a sterile cotton-tip applicator. A syringe containing a dose of 10 to 13 million VX2 sarcoma tumor cells (M.D. Anderson Cancer Center, University of Texas, Houston, Tex) excised and prepared for suspension from rabbits with primary tumors was used to inject the cells into the chest cavity adjacent to the abraded pleural surface.

Hematogenous tumor implantation. Hematogenous lung metastases were induced either by means of direct intravenous injection of the tumor cells into the rabbit ear vein or by means of intramuscular injection into the left thigh (10-15 million cells) in 12 New Zealand White rabbits. Hematogenous tumor spread to the lungs generally occurred 2 to 4 weeks after intravenous or intramuscular injection.

OCT and Flexible Fiberoptic Probe Prototype

OCT theory has been discussed in detail in previous studies.[3] in brief, OCT uses a broadband near-infrared light source in which the emitted light is split into sample and reference beams. The reflected waveforms combine to create an interference pattern (Figure E1, *a*). A low temporal coherence SLD light source (central wavelength $\lambda o = 1300$ nm and full width at half maximum = $\Delta\lambda = 80$ nm; AFC Technologies, Hull, Quebec, Canada) is connected to a Michelson interferometer that splits the light source into a sample and reference beam. These reflected beams recombine at the fiber coupler in the interferometer, producing the interference pattern detected by a photomultiplier.

Signal processing and data acquisition are accomplished with the use of a computer. Cross-sectional images were constructed by repeating the measurements at adjacent points along a sampling line. Imaging depth was approximately 1 to 2 mm. Because the OCT light source is not visible, an aiming beam (laser diode with $\lambda = 650$ nm) was coupled to the system to elucidate the location of the sampling site.

Flexible fiberoptic OCT probes (Figure E1, *b*) were constructed from single-mode fiber patch cord (ThorLabs, Newton, NJ). The bare-ended fiber was attached to a 0.5-mm-diameter GRIN lens (NSG America, Irvine, Calif) with optical adhesive (Optical Adhesive no. 68; Norland Products, Cranbury, NJ) under a microscope. A right-angle light path was achieved by using a 0.5-mm

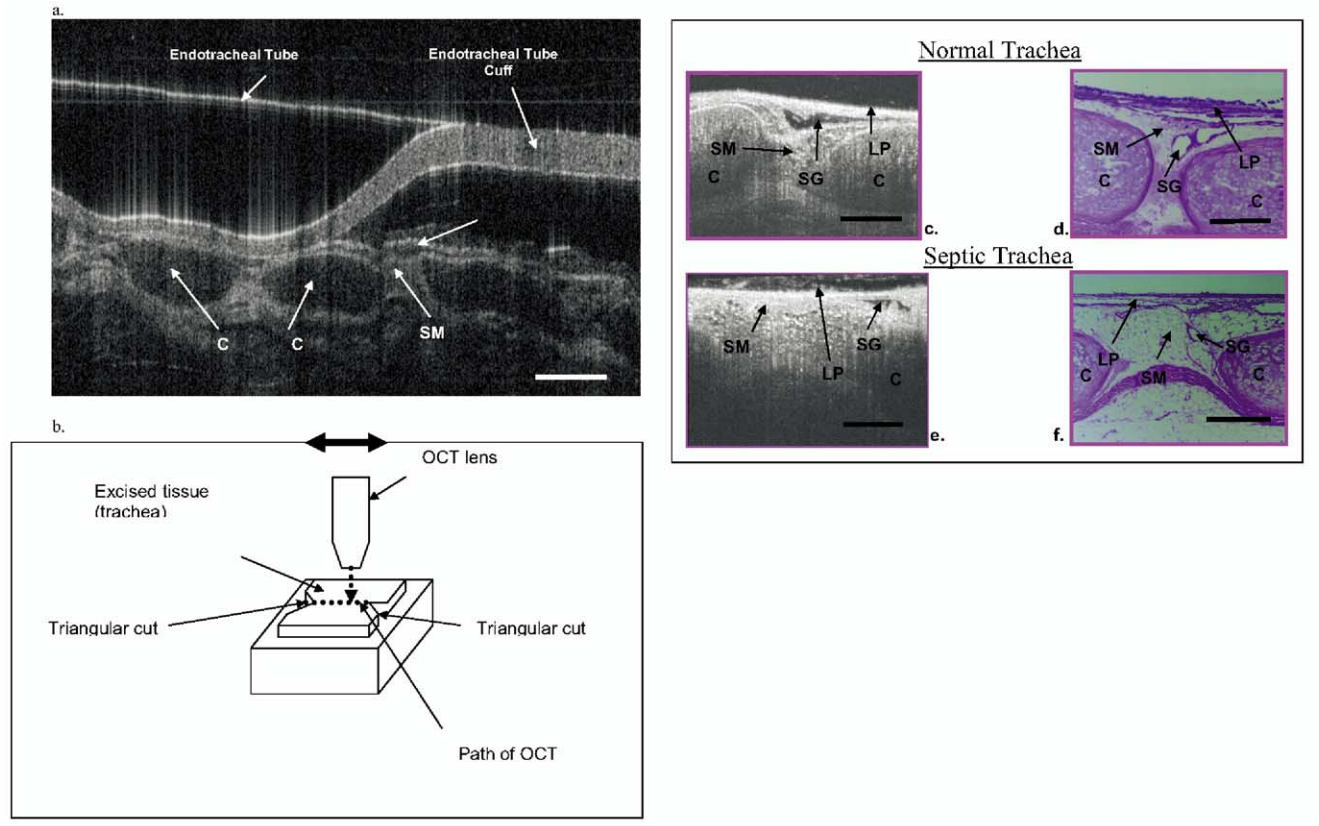

Figure 1. In vivo endoscopic image (a) of a normal rabbit trachea through an endotracheal tube (cuff number 3.0 mm outer diameter endotracheal tube). Cartilage *(C),* lamina propria *(LP),* and submucosa *(SM)* can be observed. *Bar* = 1.0 mm. Schematic of tracheal specimen preparation (b). Normal control rabbit trachea OCT image (c), with corresponding standard H&E histology (d). Inhalation injury tracheal image (e), with corresponding standard H&E histology (f). Cartilage *(C),* submucosal glands *(SG),* lamina propria *(LP),* and submucosa *(SM)* thickening is distinguishable in both OCT and histologic images (e and f). *Bar* = 0.5 mm.

prism.[10] The probe was placed in FEP tubing (17-gauge thin wall; Zeus, Orangeburg, SC) for added fiber support.

Tracheal and Lung OCT

Tracheal OCT. After anesthesia induction and intubation, the trachea was exposed by means of blunt dissection so that localization of OCT sampling could be determined. A flexible fiberoptic probe was inserted into the endotracheal tube. The visible laser light emitted from the probe confirmed the segment of trachea under OCT investigation, and OCT images were obtained. After animal death, the trachea was removed. Twelve excised tracheas were cut open longitudinally along their musculofibrous membranes and divided into approximately 29 sections of 2 cm in length. Triangular notches were cut into the opposite ends of each specimen to delineate the line of image acquisition perpendicular to the cartilage rings (Figure 1, *b*). The tracheas were secured to pieces of cork by using metal pins placed along their perimeter and covered by a layer of KY jelly to prevent desiccation during imaging. The tracheas were placed on a moveable sample platform, and a visible-light guiding beam was used to match the line of image acquisition with the triangular marking notches.

Animal lung OCT. Normal, inflamed, and malignant tissue imaging was performed on both in vivo and excised tissue. In vivo animal studies were performed as follows. After anesthesia induction and intubation, while using standard sterile surgical procedures, a 4-mm thoracoscope was inserted into the left side of the chest to inspect the visceral and parietal pleura for pathologic tissue changes. If abnormal tissue structure was observed, a second trocar was inserted under direct visualization, and a 1-mm-diameter flexible fiberoptic OCT probe was placed over the suspected lung or chest wall pathology for OCT imaging. Once it was believed that the probe was in the proper place, the ventilator was paused briefly, and images were captured. After completion of the studies, the animal was sacrificed, a median sternotomy was performed, and the tissue was excised for histologic examination.

Two- and 3-dimensional OCT. OCT images were performed on 8 excised tissues from rabbits and purchased pig lungs during the probe developmental stage in a similar fashion to images performed during in vivo studies. Specimens were mounted on cork board, and by using a 4× objective attached to a servo motor, the coherent laser light source was focused through the lens and

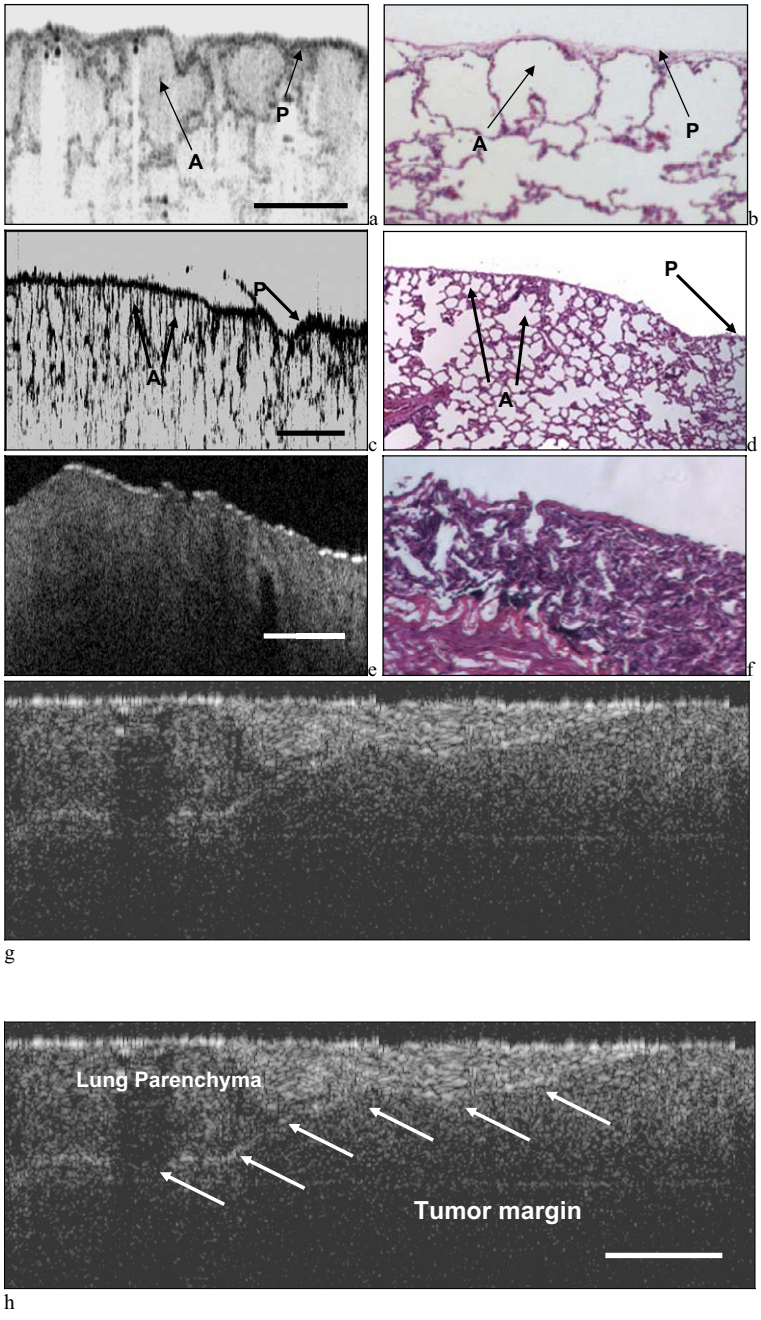

Figure 2. Normal pig lung OCT (a), with corresponding standard H&E (b). Alveoli *(A)* and pleura *(P)* can be identified in both OCT and histologic images. *Bar* = 0.5 mm. Images of normal rabbit lung by OCT (c) and corresponding standard H&E (d). As with pig lung, alveoli *(A)* and pleura *(P)* can be identified by means of both OCT and histology. *Bar* = 0.5 mm. OCT image of rabbit lung infected with *Pasteurella* species (e) and corresponding H&E (f) demonstrated pleural thickening and a lack of alveoli structures caused by purulent lung tissue. *Bar* = 0.5 mm. In vivo OCT of rabbit lung with metastatic disease without (g) and with (h) labels. *Bar* = 0.5 mm.

ET

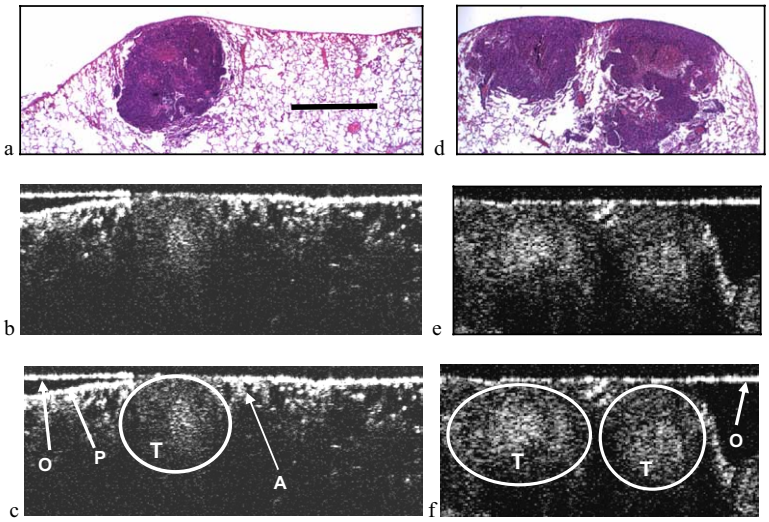

Figure 3. Histologic images of a single (a) and multiple (d) metastatic sarcoma nodules in a rabbit model. OCT images of subpleural tumors *(T)* with (b and e) and without (c and f) labels. Placement of probes *(O)* flattens the pleural *(P)* surface when imaged thoracoscopically. *Bar* = 1.0 mm.

scanned over the tissue. The specimen was advanced along the x-axis 20 or 40 μm (depending on desired resolution) after each single lateral pass on the y-axis to accomplish 3-dimensional OCT. Three-dimensional images of OCT and histology sections were constructed with the aid of a software package (3D Doctor; Able Software Corp, Lexington, Mass). The time to scan a 3-mm^3 (1 × 3 mm) tissue was approximately 20 minutes.

Human Airway OCT Imaging

During clinical bronchoscopies in patients with known or suspected airway disease, the flexible fiberoptic probe was inserted through the working channel of the bronchoscope. The suspicious region was imaged with OCT. If clinically indicated, a biopsy was performed at the imaged site and prepared in the standard manner for histologic analysis. Human studies were approved by the institutional review board (no. 2003-2907). Informed consent was obtained before bronchoscopic procedures.

Histology

Histology of excised tissue was prepared according to standard hematoxylin and eosin (H&E) histologic staining methods. OCT images and those of the histologic sections were compared. Tissue slide examination and micrographs were performed with an Olympus BH2 light microscope (Olympus American, Melville, NY) and recorded with an Olympus DP10 camera (Olympus American) for a light microscope and Olympus Digital Microfire 1.0 (Olympus American).

Results

By using the SLD prototype OCT system, 14-mm × 1.3-mm airway images were acquired and displayed in near real-time on a computer screen. High-resolution images of normal and diseased trachea, as well as normal control lung, malignant parenchymal lung tumor, visceral, parietal, and diaphragmatic pleural tumor specimens, were obtained by using OCT. These images revealed levels of resolution capable of clearly identifying airway structures, pleura, and alveoli.

Although there was variability within samples from each image, marked differences between the normal lungs and pleura compared with the malignant samples were clearly visualized with OCT. Changes ranged from loss of structure to variations in tissue thickness.

Tracheal OCT

In vivo endoscopic OCT images displayed tracheal structures visible even through the endotracheal tube (Figure 1, *a*). Clear anatomy of mucosal, submucosal, and cartilage layers are seen.

OCT images and the corresponding histology sections are shown in Figure 1, *c* and *d*, and Figure 1, *e* and *f*, for both normal and inflamed trachea, respectively. Tracheal cartilage (Figure 1, *c*) was an identifiable landmark seen during OCT imaging, which was confirmed with histology. OCT images were able to distinguish the submucosa from the lamina propria. Also observed in both OCT mapping and histology sections were submucosal glands between cartilage rings. A slight variation in tissue structure occurred, with decreased submucosal layer thickness in the histologic specimens, which was believed to have resulted from tissue property desiccation changes after excision and fixation. Injured trachea obtained from animals inoculated with *S pneumoniae* demonstrated a thickened submucosa that was seen in both OCT imaging and histology (Figure 1, *e* and *f*).

Lung and Pleural OCT

OCT imaging of lung tissue was able to detect structures as fine as alveolar septa and visceral pleura. Figure 2, *a* and *b*,

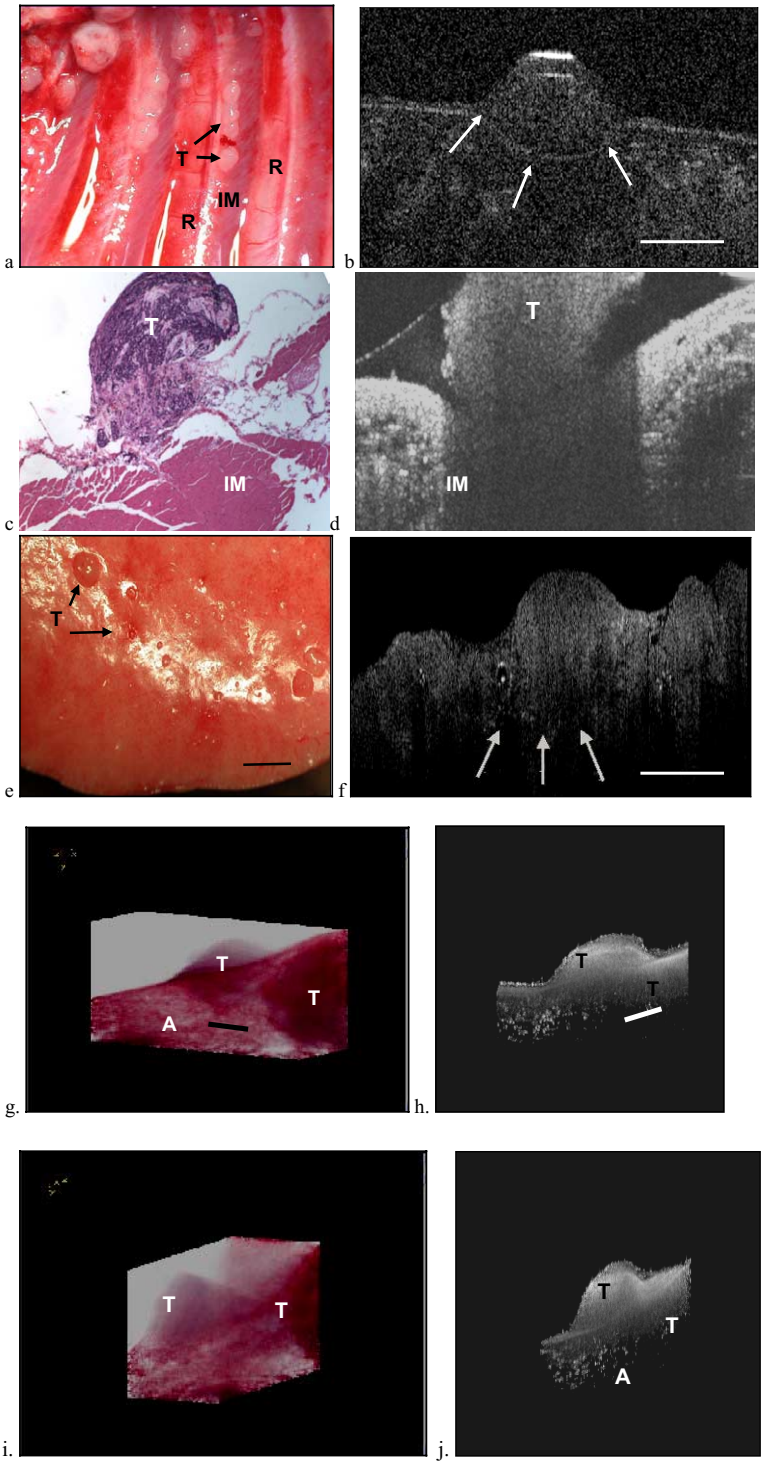

Figure 4. Gross specimen (a) of chest wall parietal pleural tumor *(T)*. Tumor nodules were interdispersed between ribs *(R)* and intercostal muscle *(IM)*. OCT of visceral pleural tumor originating from pleural space (b). Detection of a continuous pleural line *(arrows)* suggests in situ growth without invasion across adjacent tissue. *Bar* = 1.0 mm. Histology (c) and OCT (d) of chest wall parietal pleural tumor *(T)*. Shadowing of the tumor occurs when high absorption-reflection surfaces effectively block further penetration of light interference below them. Gross specimen (e) of lung visceral pleural tumor *(T)*. Notable variations in tumor growth were apparent. *Bar* = 5.0 mm. OCT of visceral pleural tumor (f). Absence of pleural line below tumor suggests hematogenous origin of this metastatic tumor. *Bar* = 0.5 mm. Three-dimensional histology (g and i) and OCT (h and j). Three-dimensional reconstruction of histology and OCT shows 2 tumor nodules *(T)* and normal tissue where alveoli *(A)* can be identified. *Bar* = 0.5 mm.

and Figure 2, *c* and *d*, show comparisons between OCT and histology of normal pig and rabbit lung specimens, respectively. In Figure 2 alveoli and visceral pleura were discernible. OCT images of pig lung are superior to those of rabbit lung, possibly because of the finer structures in the rabbit lung. However, in the rabbit lung tissue with induced bacterial empyema (Figure 2, *e*) and metastatic disease (Figure 2, *g* and *h*), these structures were no longer distinguishable because of thickening of the pleura and filling of the alveoli with purulent material (Figure 2, *f*) and the compression of adjacent tissues by lung tumor Figure 3.

In vivo thoracoscopic examination revealed subpleural tumors (Figure 3), although detection of lung malignancies at increasing tissue depth (>2-3 mm) was not possible. Lung tumors as small as 500 μm (Figure 4, *e*), which were difficult to detect by means of gross examination, could be observed with OCT (Figure 4, *f*).

Small parietal (Figure 4, *a*, *c*, and *d*) and visceral (Figure 4, *b*, and *e*) pleural-based tumors that had not invaded the parenchyma could be characterized by means of visualization of the pleural line below the nodule (Figure 4, *b*). In contrast, small hematogenous tumor metastases that formed below the pleural surface showed very different characteristics on OCT (Figure 4, *f*).

Three-Dimensional Imaging of OCT

In selected specimens 3-dimensional reconstructions were prepared and analyzed for comparison with 3-dimensional histology. Although some differences caused by fixation of the histologic slide tissues were noted, both OCT and histologic 3-dimensional images demonstrated very similar appearance. Figure 4, *g* through *j*, shows 3-dimensional relationships between OCT images and histologic preparations.

Human Airway

Two patients with and without airway disease who provided informed consent (protocol HS#2003-2907) underwent clinical flexible fiberoptic bronchoscopies with OCT. The OCT probe was passed through the working port of the flexible fiberoptic bronchoscope, and OCT images were obtained of the intrabronchial lesions. Lateral scanning sampling resolution averaged 20 to 30 μm in the lung. Images showed changes in airway structure in malignant airway regions when compared with normal tissue. Pathologic changes noted on OCT consisted of a thickened mucosa and disorganization of tracheal tissue layers when compared with sections of normal tissue. Corresponding OCT and white-light bronchoscope images of inflamed tissues obtained during bronchoscopy are shown in Figure 5.

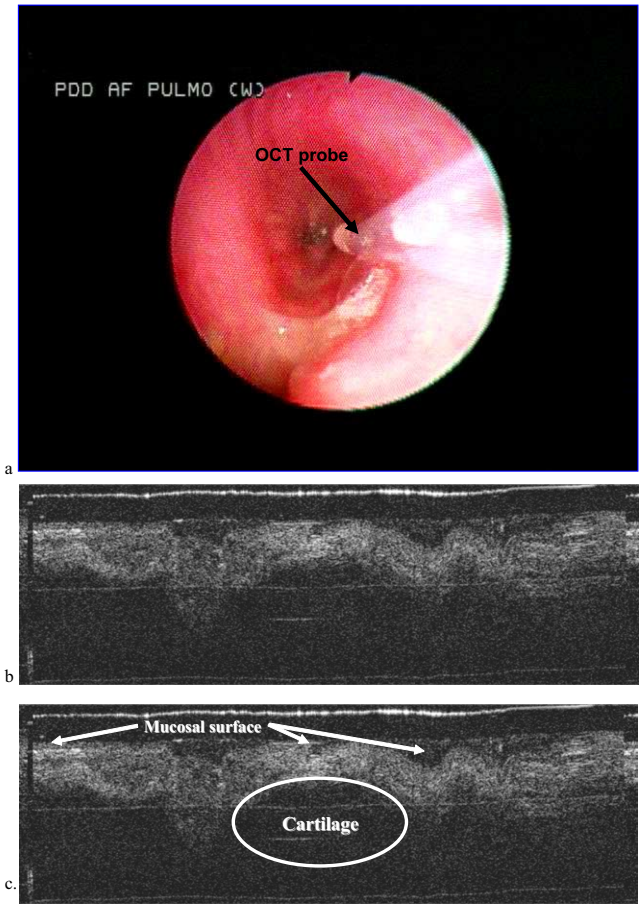

Figure 5. Image (a) of an OCT probe *(O)* within a human airway (right upper lobe bronchus) obtained through a flexible fiber bronchoscope. In vivo OCT image of an inflamed right upper lobe bronchus without (b) and with (c) labels.

Discussion

These studies confirm the feasibility of high-resolution OCT imaging of the airway and pleura for evaluating distal airway, lung, and pleural pathology to obtain optical images at near-histologic levels in vivo. Differences in tissue layers of the airway and pleura were clearly distinguishable and corresponded closely to standard H&E images subsequently obtained from the excised tissues. OCT images could be obtained in near real time in vivo with the use of flexible fiberoptic probes and applied to the clinical setting. To our knowledge, this is the first report of high-resolution, in vivo, bronchoscopic OCT imaging in diseased human bronchi imaged by means of OCT during flexible fiberoptic bronchoscopy. Previous medical applications exploring the use of OCT have been investigated in the fields of ophthalmology, gastroenterology, and cardiology.[11-16] There are many areas of thoracic clinical diagnosis in which OCT might become useful as resolution improves. Recent studies in our own and affiliated laboratories[8] have demonstrated OCT capabilities in proximal airways in ex vivo specimens. With the availability of in vivo high-resolution optical capabilities, responses to therapy in thoracic diseases might be

ET

better assessed in addition to improved diagnosis. At the current level of actual resolution (10-20 μm), tissue layers, mucosa, and airway epithelium were visualized. Architectural disruptions in diseased tracheal specimens (Figure 1, *d*) clearly demonstrated an increase in mucosal thickness that suggested underlying tissue damage. In airway inhalation injury delineation of submucosal edema, hyperemia, and blood flow changes by OCT (including use of optical Doppler tomographic techniques)[17] could become a significant adjunct to bronchoscopy for the management of tracheal and bronchial injury.

Histologic examination of bronchial mucosa during flexible or rigid bronchoscopic procedures could greatly assist in the diagnosis and localization of endobronchial malignancy. This might be particularly useful in malignancies such as adenoid cystic carcinomas in which tumor spread tends to occur in the submucosal plane well beyond the observed luminal component of the tumor. Application of OCT in this and similar settings would allow for possible detection of hidden margins (Figure 2, *g*) that might otherwise be missed in gross examination and could assist with guiding resection margins, as well as assessing operability.

Tissue structural changes strongly suggestive of malignant tumor invasion could be detected at resolution of the current SLD OCT system (Figure 4). However, improvement in resolution to 1 to 2 μm will be required to visualize nuclei and organelles to definitively differentiate malignant transformation optically at a cellular level. Such improvements in resolution might be achievable in the near future by using broadband light sources, polarization-sensitive OCT (PS-OCT), and multiphoton microscopy combined with OCT.[18]

The ability to visualize tissue structures in real time at a near-histologic level of resolution opens up a wide range of potential areas for clinical and research applications in thoracic surgery. In the future, when cellular-level OCT resolutions are obtained, even greater uses for OCT in thoracic diagnostics can be envisioned. However, the depth of penetration of OCT is relatively shallow (1-2 mm) and is likely to remain limited by the degree of scattering inherent in complex biologic tissues of the lung and thorax, and thus major advances in depth of penetration are unlikely. Nevertheless, there are many scenarios in thoracic surgery in which surface and near-surface, in vivo, high-resolution optical imaging are of great potential value.

The development of 3-dimensional high-resolution OCT probes, endoscopes, and image-processing and display technologies might allow for improved assessment of tumor margins and detection of satellite lesions. Further into the future, very small OCT probes could be designed to fit within needles to allow imaging at depths within masses with near real-time histologic resolution capabilities.

This study has demonstrated the feasibility of high-resolution 2- and 3-dimensional OCT for examination of thoracic airway and pleural abnormalities. There are a range of potential research and clinical applications for OCT imaging in thoracic surgery and diagnostics. The technology used in this study is limited to 10- to 30-μm resolutions, and depth of penetration is generally a maximum of 2 to 3 mm. With further improvement in resolution, contrast, acquisition, display, and processing and the development of specific thoracic probes, OCT might offer a significant advance for the diagnosis and treatment of patients with thoracic diseases.

We thank Hamza Beydoun, Jenny Armstrong, Teri-Waite, Larry Cherrison, and Tanya Burney for their technical assistance. We also thank Brian Jordan, Dr Andrey Yershov, and Dr Ronald Walton at the Institute of Surgical Research, Brook Army Medical Center, San Antonio, Tex, for their supply of tracheal specimens.

References

1. Hunt JL, Agee RN, Pruitt BA Jr. Fiberoptic bronchoscopy in acute inhalation injury. *J Trauma.* 1975;15:641-9.
2. Paul S, Bueno R. The burned trachea. *Chest Surg Clin N Am.* 2003; 13:343-8.
3. Huang D, Swanson EA, Lin CP, et al. Optical coherence tomography. *Science.* 1991;254:1178-81.
4. Fujimoto JG, Brezinski ME, Tearney GJ, et al. Optical biopsy and imaging using optical coherence tomography. *Nat Med.* 1995;1:970-2.
5. Hitzenberger CK, Danner M, Drexler W, et al. Measurement of the spatial coherence of superluminescent diodes. *J Modern Opt.* 1999; 46:1763-74.
6. Park BH, Saxer C, Srinivas SM, et al. In vivo burn depth determination by high-speed fiber-based polarization sensitive optical coherence tomography. *J Biomed Opt.* 2001;6:474-9.
7. Herrmann JM, Brezinski ME, Bouma BE, et al. Two- and three-dimensional high-resolution imaging of the human oviduct with optical coherence tomography. *Fertil Steril.* 1998;70:155-8.
8. Jung W, Zhang J, Mina-Araghi R, et al. Feasibility study of normal and septic tracheal imaging using optical coherence tomography. *Lasers Surg Med.* 2004;35:121-7.
9. Sasse SA, Causing LA, Mulligan ME, et al. Serial pleural fluid analysis in a new experimental model of empyema. *Chest.* 1996;109: 1043-8.
10. Bouma BE, Tearney GJ. Power-efficient nonreciprocal interferometer and linear-scanning fiber-optic catheter for optical coherence tomography. *Opt Lett.* 1999;24:531-3.
11. Jackle S, Gladkova N, Feldchtein F, et al. In vivo endoscopic optical coherence tomography of esophagitis, Barrett's esophagus, and adenocarcinoma of the esophagus. *Endoscopy.* 2000;32:750-5.
12. Pitris C, Jesser C, Boppart SA, et al. Feasibility of optical coherence tomography for high-resolution imaging of human gastrointestinal tract malignancies. *J Gastroenterol.* 2000;35:87-92.
13. Brezinski ME, Tearney GJ, Weissman NJ, et al. Assessing atherosclerotic plaque morphology: comparison of optical coherence tomography and high frequency intravascular ultrasound. *Heart.* 1997;77:397-403.
14. Yabushita H, Bouma BE, Houser SL, et al. Characterization of human atherosclerosis by optical coherence tomography. *Circulation.* 2002; 106:1640-5.
15. Brezinski M. Characterizing arterial plaque with optical coherence tomography. *Curr Opin Cardiol.* 2002;17:648-55.
16. Tearney GJ, Yabushita H, Houser SL, et al. Quantification of macrophage content in atherosclerotic plaques by optical coherence tomography. *Circulation.* 2003;107:113-9.
17. Kehlet Barton J, Izatt JA, Kulkarni MD, et al. Three-dimensional reconstruction of blood vessels from in vivo color Doppler optical coherence tomography images. *Dermatology.* 1999;198:355-61.
18. Yeh AT, Kao B, Jung WG, et al. Imaging wound healing using optical coherence tomography and multiphoton microscopy in an in vitro skin-equivalent tissue model. *J Biomed Opt.* 2004;9:248-53.

ET

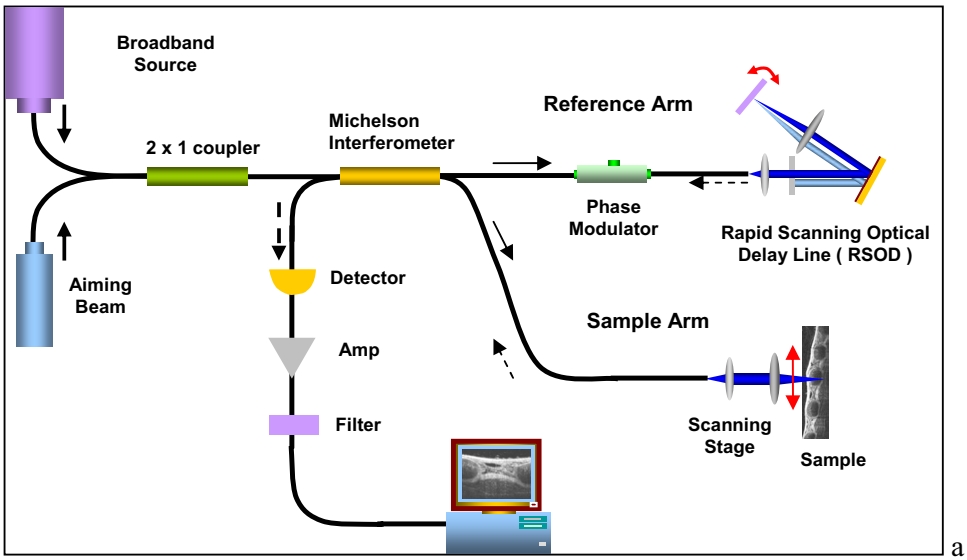

a

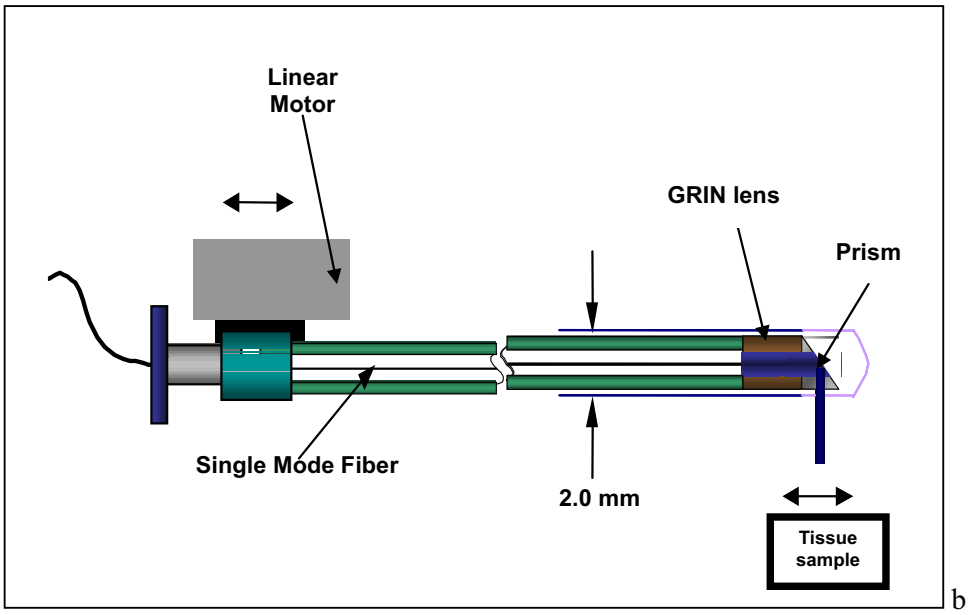

b

Figure E1. a, OCT schematic. Light from a coherent broadband source is coupled with an aiming beam at an inverted 2 × 1 beam splitter. The beam is split at the Michelson interferometer into reference and sampling beams. The reflected wave forms are then recombined at the interferometer, digitally processed, and displayed as a gray scale map. b, Translational endoscopic OCT probe for in vivo imaging. A prism and lens are attached to single-mode fiber. The distal end of the fiber is attached to a linear motor, and the proximal end of the probe is enclosed in tubing with an outside diameter of 2.0 mm.